Tilt bifurcation and dynamical selection by tilt domains in thin-film lamellar eutectic growth: Experimental evidence of a tilt bifurcation

G. Faivre and J. Mergy
Groupe de Physique des Solides, Universités Paris 7 et Pierre et Marie Curie, Tour 23, 2 place Jussieu, 75251 Paris CEDEX 05, France
(Received 9 December 1991)

In thin-film directional solidification of the CBr_4-C_2Cl_6 eutectic alloy, we observe a quasi-instantaneous transition from symmetric states to drifting parity-broken ("tilted") states as a result of a sudden increase of the pulling velocity. We show that (i) the observed transition is essentially the forward-tilt bifurcation that Kassner and Misbah [Phys. Rev. Lett. **65**, 1458 (1990); **66**, 522 (1991)] have recently found, numerically, in a model without anisotropy of the solid phases; (ii) crystal anisotropy, in the eutectic system, makes the bifurcation slightly imperfect. In lamellar eutectics, phase diffusion is extremely slow, and permanent spatial modulations of the pattern wavelength are always present, generated at eutectic grain boundaries. We show that the tilt angle, i.e., the degree of parity breaking of the pattern, adjusts itself locally to the wavelength in a very short time, in contrast with the slow phase diffusion.

PACS number(s): 81.10.Fq, 64.70.Dv, 03.40.−t

I. INTRODUCTION

The symmetric, stationary, periodic patterns of directional solidification fronts can, under some conditions, break their symmetry with respect to the growth direction (i.e., the parity of their front profile with respect to the coordinate perpendicular to the modulation; see Fig. 1) and switch to asymmetric patterns drifting along the front. The existence of this possibility and its implications for the dynamics of cellular fronts, especially as regards the well-known [1] wavelength-selection problem, have been fully recognized only recently. To our knowledge, attention was first drawn to the parity-breaking or "tilt" instability [in the context of eutectics, the latter term is more suggestive (see Fig. 1) and will be used thereafter] by the observation of small domains of tilted cells on a nematic-isotropic directional solidification front by Simon, Bechhoefer, and Libchaber [2]. Traveling sideways along the front, these "tilt domains" erase the preexisting symmetric ("untilted") cellular pattern and leave behind them a new untilted pattern, which, under certain conditions, has an average value and a distribution of its wavelength different from those of the preexisting one. A similar observation was made by other authors on a lamellar eutectic solidification front [3], and on a hydrodynamic analog of directional solidification fronts [4], attesting to the generic character of these dynamical "objects."

The following was almost immediately inferred from these observations, in particular by Coullet, Goldstein, and Gunaratne [5].

(1) The system is likely to have a bifurcation from space-filling ("extended") stationary untilted states to tilted ones.

(2) The emission and propagation of tilt domains is a wavelength-selecting mechanism of a particular type; a convincing phenomenological model of this "dynamical selection," based on the assumption of a tilt bifurcation, was devised by Coullet, Goldstein, and Gunaratne [5] and further improved by Goldstein *et al.* [6] and Caroli, Caroli, and Fauve [7].

Direct experimental evidence for the tilt bifurcation has been lacking, however. In this article, we present such evidence, which we have obtained on the system where we had previously observed tilt domains [3] (called tilt waves in that first report): the lamellar eutectic alloy CBr_4-C_2Cl_6, directionally solidified in thin films. We have also carried out a detailed investigation of the dynamical wavelength selection by tilt domains in this system; those results are planned to be presented in a further article (hereafter, we refer to this article as paper II).

The well-known geometry and setup [8–10] of thin-

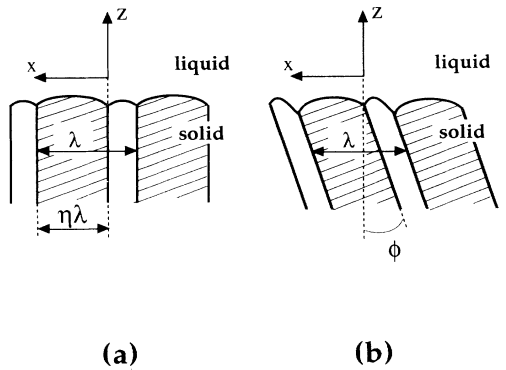

FIG. 1. (a) Symmetric "untilted" stationary state of directionally solidified lamellar eutectics. The lamellae of one of the two solid phases are hatched (in the case shown, the volume fraction of this phase is $\eta=0.7$). Oz is the pulling or growth direction (see Fig. 2), Ox the lateral, and Oy (not shown) the transverse direction. (b) Generic "tilted" stationary state. The pattern drifts in the lateral direction, leaving behind lamellae with the tilt angle ϕ.

 ©1992 The American Physical Society

film directional solidification experiments is sketched in Fig. 2. The transparent eutectic alloy $CBr_4C_2Cl_6$ has been studied by many researchers [8,9,11,12], but only recently with the view of investigating its dynamical behavior as such. The dynamics of this system is rich, including, in particular, several oscillating regimes (see Ref. [13] for a rapid survey). For clarity, we shall focus here, as much as possible, on the parity-breaking instabilities only.

In the search for the tilt bifurcation, we were guided by the recent theoretical findings of Kassner and Misbah [14–16]. They assume a "minimal" model, minimal meaning here that they make all the simplifying assumptions that are reasonable in a first approach to thin-film directional solidification [17]. Of particular importance for what follows is that crystal anisotropy is ignored: all interfacial energies are supposed isotropic (orientation independent).

At fixed thermal gradient G and alloy concentration C, the pulling velocity V is the only control parameter of the system. The possible lateral drift of the pattern being taken into account, two variables are needed, at given V, to parametrize all the conceivable periodic stationary states of the system, e.g., the wavelength λ and the tilt angle ϕ—it being understood that a tilted ($\phi \neq 0$) pattern is stationary not in the laboratory reference frame but in a frame drifting sideways at velocity $V_x = V\tan\phi$ [see Fig. 1(b)]. It has been shown by Brattkus *et al.* [18] that, for given V and λ, the minimal model cannot admit a continuum (in the variable ϕ) of stationary periodic solutions: it can at most have a discrete set of solutions, including the untilted solution $\phi = 0$. Kassner and Misbah, integrating numerically the equations of the minimal model for material parameters corresponding to the CBr_4-C_2Cl_6 system, have established the following results.

(1) For a given wavelength λ, extended tilted states appear via a forward bifurcation from the untilted states at a critical pulling velocity V_T.

(2) In accordance with previously established similarity relations [14], the bifurcation diagram can in fact be plotted, to a first approximation, as a function of the parameter $\lambda^2 V$ (Fig. 3). The essential condition for this assertion to be valid is a small Péclet number $\mathrm{Pe} = \lambda/l$, where $l = D/V$ is the diffusion length and D is the chemical diffusion coefficient of the solute in the liquid. The condition is clearly fulfilled in the experiments reported below ($D \simeq 500\ \mu\mathrm{m}^2\,\mathrm{s}^{-1}$ [19], $V < 4.3\ \mu\mathrm{m\,s}^{-1}$, $\lambda < 16\ \mu\mathrm{m}$, so $\mathrm{Pe} < 0.15$). Then, the exact statement is as follows: ϕ is a function of two variables, $\lambda^2 V$ and G/V, but the dependence on G/V becomes negligible when this ratio is much smaller than a certain value which for our system, is of the order of $0.02\ \mu\mathrm{m}^{-2}\,\mathrm{s\,K}$. In our experiments, G/V is less than $0.01\ \mu\mathrm{m}^{-2}\,\mathrm{s\,K}$.

(3) The steepness of the tilted branch near the bifurcation threshold is primarily determined by the ratio d/l of the capillary to the diffusion length. In our experiments, $d \cong 10^{-2}\ \mu\mathrm{m}$ [19], so that $d/l < 10^{-4}$; as a consequence, the tilt bifurcation is very steep: for $\lambda^2 V$ a few percent above the critical value, ϕ is about 25°.

(4) The critical value $(\lambda^2 V)_T$ for the tilt bifurcation is about 4 times larger than the Jackson-Hunt [9] minimum-undercooling value $(\lambda^2 V)_m = \lambda_m^2(V)V$. Since $\lambda_m(V)$ varies as $V^{-1/2}$, we can state equivalently that the λ threshold at given pulling velocity is approximately $2\lambda_m$.

The experimental procedure prescribed by these theoretical results is, in principle, straightforward. The most well-known (but unexplained) observation concerning lamellar eutectics is that, when pulled at a fixed velocity for a long time, they stabilize in the untilted periodic pattern with a more or less closely selected wavelength near the minimum-undercooling value for that velocity [9,20]. The procedure we used is then simply, first, to pull the sample at some velocity V_1 for a time long enough for the system to stabilize in the untilted pattern of wavelength $\lambda_{m1} = \lambda_m(V_1)$; second, to switch the pulling velocity to a value $V_2 = RV_1$, with $R > 1$. According to the bifurcation diagram in Fig. 3, when $R > R_T \cong 4$, and on condition that the number of lamellae be conserved during the transient, the system should become unstable and subsequently restabilize in the tilted pattern of wavelength λ_{m1} and tilt angle $\tilde{\phi}(\lambda_{m1}^2 V_2)$, where $\tilde{\phi}$ denotes the value of ϕ in the stationary states represented

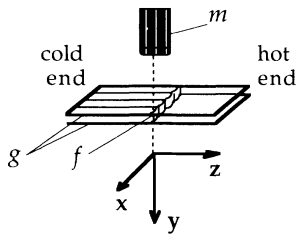

FIG. 2. Thin-film directional solidification setup. A film of a transparent alloy, enclosed between two parallel glass plates (g) is placed in a fixed thermal gradient (directed along Oz). The sample is pulled at velocity V in the Oz direction. The position of the solid-liquid front (f) is fixed in the laboratory frame, and moves at the imposed velocity V with respect to the liquid. The front is observed with an optical microscope (m) connected with a videotape recorder.

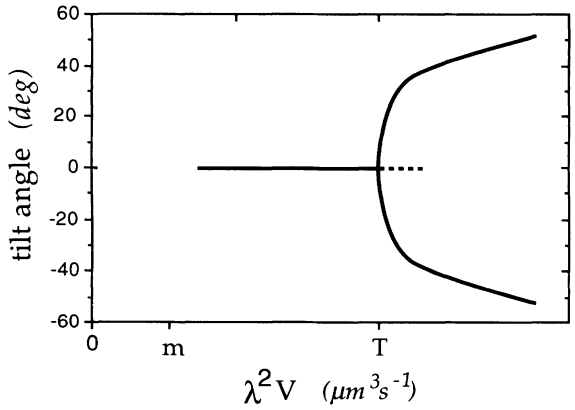

FIG. 3. The tilt bifurcation as calculated by Kassner and Misbah [16] (sketch); m: minimum undercooling; T: bifurcation threshold.

by the solid lines in the bifurcation diagram of Fig. 3; it should not do so when $R > R_T$. This is essentially what is observed, as we shall show shortly. However, the behavior of the real system is more complicated than that implied by this simplified vision. The significant additional complexities have two sources: the extreme slowness of phase diffusion and the presence of surface-tension anisotropy. The conjunction of these two features results, in particular, in permanent gradients of the local wavelength (often termed lamellar spacing in the case of eutectics; similarly, the "cell" is called the pair of lamellae). To make this article self-contained, we summarize our recent findings on this subject [21].

(1) The growth fronts of our samples are always composed of "eutectic grains," i.e., regions of homogeneous crystal orientation of the two solid phases. The action of surface-tension anisotropy, whatever its nature and strength, is uniform within a grain, and different in different grains.

(2) There are two distinct types of eutectic grains depending on whether the generalized Wulff plot of the $\alpha\beta$ interphase interface is smooth or has cusp singularities. We shall be concerned here only with the first case, which we have called "floating grains." For these grains, surface-tension anisotropy acts as a smooth, weak perturbation of the ideal system represented by the minimal model. For the other type of grains, the "locked" grains, surface-tension anisotropy is strong enough to lock the $\alpha\beta$ interfaces onto singular epitaxy directions.

(3) For floating eutectic grains, the generic situation is that surface-tension anisotropy breaks the parity symmetry of the system. Then, even the basic stationary states, i.e., those states that would be untilted in the absence of anisotropy, are slightly inclined by an angle ϕ_0, which is a function of the particular orientation of the grain. The value of ϕ_0 is found to be at most 5° in basic states with λ close to λ_m.

(4) A straightforward consequence of point 3 is that a perfectly uniform basic state cannot exist in a sample containing several eutectic grains. At the boundary between two adjacent (floating) eutectic grains, the lamellae of one grain are constrained to run towards (away from) the lamellae of the other grain, if the boundary is "converging" ("diverging"), i.e., if the difference of the ϕ_0 values in the two grains is negative (positive). The system reacts to this constraint in a variety of ways, but, because phase diffusion is ineffective, the net result is that a trough or bump of the λ distribution is permanently attached to each boundary, extending typically over 10 pairs of lamellae on both sides of the boundary. This is, at least in our samples the main origin of the well-known (see, e.g., [12]) basic-state irreducible 10–20 % λ dispersion of the "selected" wavelength.

II. EXPERIMENTAL PROCEDURES

The description of the thin-film directional solidification setup we used can be found in other places [22,23]. The two parallel glass plates containing the crystallizing film (Fig. 2) also ensure the conduction of the heat from the hot to the cold end of the sample. The temperature profile at the growth front has been measured with a thermocouple. It is satisfactorily linear and stable when the pulling velocity is kept constant, but shifts slightly towards the cold end when the pulling velocity is suddenly increased. It takes about 10 s for the temperature to stabilize to its new profile. The velocity jumps of the growth front are smoothed by this effect. In practice, this means that the conditions during the first 10 s or so of the post-jump transients are relatively ill defined.

We used here very thin (≈ 16 μm thick along Oy) and wide (≈ 6 mm wide along Oz) samples. By very thin, we mean a thickness comparable with, or smaller, than the lamellar spacings in the pattern. This specification is important and demands some explanation. It has to do with the above-mentioned condition that the average wavelength be kept constant, thus that no lamella be created during the transients. We shall give elsewhere experimental evidence that tip splitting is not, in lamellar eutectics, the mechanism by which new lamellae are created. The nature and conditions of occurrence of the lamellar-birth mechanism have not yet been studied in detail. There seem to exist two types of instability from which a lamellar birth can result. Both are "transverse," implying a distortion of the preexisting lamellae in the Oy direction [24]. One of them is local (i.e., involves one pair of lamellae only) and has a λ threshold $> 2\lambda_m$. The other is extended and can occur at $\lambda < \lambda_m$. To allow the tilt bifurcation to take place, the latter instability must be prevented. This condition is clearly more easily fulfilled in very thin samples, thanks, probably, to the stabilizing effect of the wetting forces at the glass plates [25].

Two more issues turned out to be, in practice, crucial: first, the purity of the alloy; second, the size of the eutectic grains. Residual impurities play a role in the well-known cellular-dendritic instability that occurs in impure and/or off-eutectic alloys at high pulling velocity [26]. In our carefully purified samples [19], the threshold for this instability, in the extended tilted state, was observed at ~ 5 μm s^{-1}. When V_2 is lower than this value, the tilted state is apparently stable (see below), but dendrites nevertheless appear in certain perturbed regions, e.g., near the lateral borders of the film; these localized dendrites progressively perturb the remainder of the front (an instance is visible in the upper left corner of Fig. 5.) This limits the utilizable range of values of V_2 and the period of time available for the study of the dynamics in the extended tilted state.

Grain-boundary effects, as explained above, clearly imply that samples containing wide floating grains are needed. In practice, grains containing ~ 100 lamellar spacings turned out to be required. Currently, this specification is hard to fulfill [27].

On the other hand, the precise values of the thermal gradient and the concentration of the alloy are of secondary importance for our present purpose, provided that they are kept constant from one experimental run to the other. The tilt phenomena being most easily triggered at hypereutectic concentrations [13], the experiments were done with C near the center of the eutectic plateau. The *in situ* measured volume fraction of the α phase was

TABLE I. The four successive runs of the experiment described in the text. V_1 and V_2 are the pulling velocities before and after the velocity jump, respectively.

Run	V_1 ($\mu m\,s^{-1}$) ± 0.05	V_2 ($\mu m\,s^{-1}$) ± 0.2	$R = V_2/V_1$ ± 0.2
1	0.85	3.3	3.9
2	0.85	3.6	4.2
3	0.85	4.1	4.8
4	0.85	4.4	5.2

$\eta = 0.5 \pm 0.02$ (the eutectic point of the CBr_4-C_2Cl_6 alloy is about $\eta = 0.7$). The thermal gradient was $G = 80 + 5$ K cm^{-1}.

All the samples examined have given very similar results concerning the tilt bifurcation. Let us, for clarity, describe one particular experiment, from which most of the photographs shown in this article have been taken. A 16-μm-thick, 6-mm-wide sample, filled with an $\eta = \frac{1}{2}$ alloy, was placed in the temperature gradient $G = 80$ K cm^{-1}, in a position where the film was almost completely liquid. It was maintained in this position for about 1 h. The pulling was switched on, at velocity $V_1 = 0.85$ $\mu m\,s^{-1}$, and maintained at this velocity until an apparently homogeneous basic-state lamellar structure was established within the widest eutectic grains. This took approximately 0.5 h. The velocity was then switched to $V_2 = 3.3$ $\mu m\,s^{-1}$. After a certain time of pulling at V_2, the velocity was switched back to zero. The whole procedure was then repeated, with a different value of V_2. Four values of V_2, hence of the ratio $R = V_2/V_1$, were explored in a row (Table I) before reaching the end of the sample. The reproducibility of the "initial state," i.e., the state at the time of the jump (thereafter taken as time $t = 0$ and denoted by the index 0) was tested in several ways against possible drifts of the concentration. A good test is, for instance, the normalized λ_0 histogram of the system, shown in Fig. 4, for the four runs. The reproducibility is satisfactory. The long tail towards high λ values is a manifestation of the grain-boundary effects; the fact that, in the case of run 1, it takes on the form of a secondary maximum denotes only an accidentally large number of small grains (the grains were not conserved from one run to the next one).

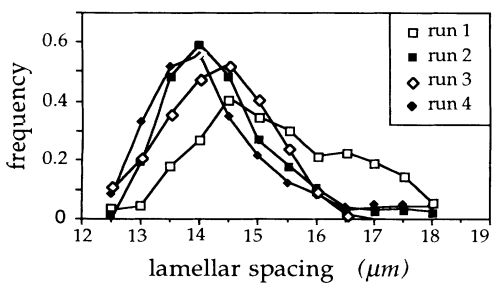

FIG. 4. Histograms of the lamellar spacings in the initial untilted states of the four runs listed in Table I.

FIG. 5. Velocity jump from $V_1 = 0.85$ to $V_2 = 3.6$ $\mu m\,s^{-1}$ (run 2 of Table I). Photograph of the solid (the solidification front is out of the image). Time is running upwards. Arrows: velocity jump ($t = 0$). Bar: 200 μm. Numbers 1–4: eutectic grains. The values of ϕ_0 for grains 1–4 are $+3°$, $-2°$, $+2.5°$, $-1.5°$, respectively. An incipient dendritic destablization is visible in the upper left corner as are "sources" emitting tilted lamellae at the 1–2 and 3–4 grain boundaries (sources and other "defects" of the tilted state will be described in paper II).

III. RESULTS

A. Evidence of a tilt bifurcation

The four velocity jumps of ratio $R \geq 4$ listed in Table I all resulted in a quasihomogeneous tilting of the preexisting pattern. Figures 5 and 6 show photographs of regions of the solid corresponding to the velocity jumps 2 and 3 of Table I, i.e., to jumps of amplitudes $R = 4.2$ and 4.8, respectively. Let us explain, with the help of Fig. 7, how such images are to be read. The photograph in Fig. 7 was taken during the course of the pulling, a few seconds after the velocity had been switched to V_2. In Fig. 6, the same region has been photographed much later, after the pulling had been stopped. It is evident in Fig. 7 that the $\alpha\beta$ interfaces in the solid give a time history of the trajectories of the triple points where the α, β, and liquid phases meet. Because of the extreme slowness of diffusion in the solid, no change is perceptible from Fig. 7 to Fig. 6. Thus, a photograph of a region of the solid, irrespective of how far behind the front it lies, can be read as a set of trajectories of triple points, i.e., a spatiotemporal diagram of the system evolution. Similarly, we can obtain the $\lambda(x)$ distribution of the system at any time by taking the corresponding cross section along Ox of such images.

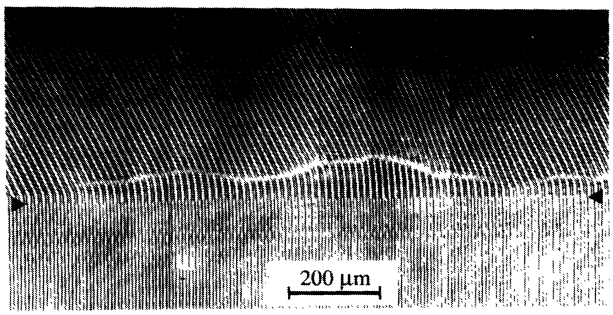

FIG. 6. Velocity jump from $V_1 = 0.85$ to $V_2 = 4.1$ $\mu m\,s^{-1}$ (run 3 of Table I). See Fig. 5 for explanations. Only one eutectic grain is visible in the image ($\phi_0 = +0.5°$).

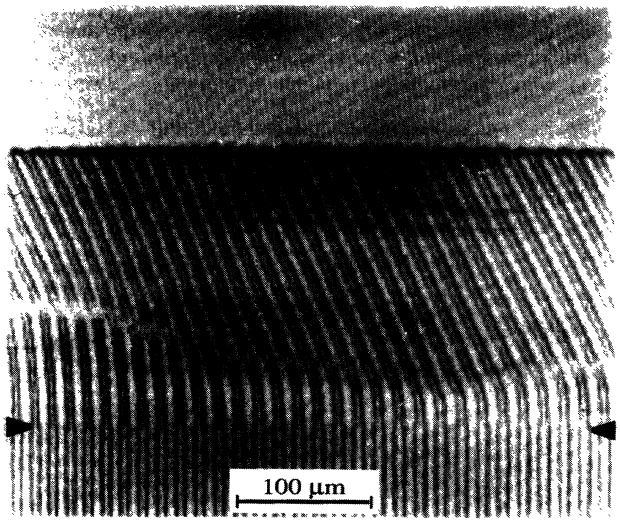

FIG. 7. Enlarged view of the same region as in Fig. 6. The photograph was taken at $t = 65$ s.

It can be seen in Figs. 5 and 6 that large domains of the basic state change very rapidly (but not instantaneously) to a quasihomogeneous, apparently stable, strongly tilted state as a result of the sudden increase of the pulling velocity by factor ≥ 4. No lamella is created or destroyed in the process. The lateral extension of the domains is limited only by extrinsic factors, in fact by eutectic grain boundaries: As we shall show below, each homogeneous domain in Fig. 5, and the whole field of Fig. 6 (~ 100 lamellar spacings) corresponds to a eutectic grain. The reversible character of the tilting when the pulling velocity is switched back to its initial value is demonstrated by Fig. 8.

On the other hand, no homogeneous tilting of the basic state occurs when the amplitude of the velocity jump is

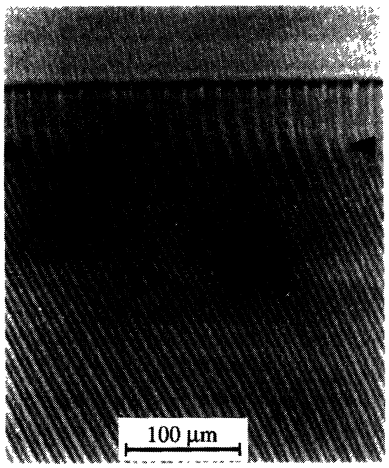

FIG. 8. Velocity jump from 4.1 to 0.85 μm s^{-1} (end of run 3). Arrows: velocity jump.

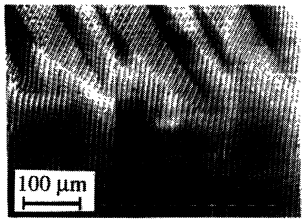

FIG. 9. Subcritical velocity jump ($V_1 = 0.85$ μm s^{-1}; $V_2 = 2.26$ μm s^{-1}; $R = 2.7$). Dashed line: velocity jump.

substantially smaller than 4. In this case, a process of nucleation and growth of tilt domains is observed (Fig. 9). Its study is beyond the scope of this article; for our present purpose, it will suffice to note that, undoubtedly, there exists a critical value of $\lambda^2 V$, close to 4, which marks the lower limit for the homogeneous transition from the basic untilted state to the tilted one. This is, essentially, the bifurcation predicted by Kassner and Misbah for the minimal model. We shall now characterize in more detail the bifurcation we actually observe.

B. The transition delay: Local character of the bifurcation

The transition to the tilted state is not instantaneous. Selecting a particular group of contiguous pairs of lamellae and following their trajectories after the velocity jump, one notes (see, in particular, Fig. 7) (i) a slight bulging of the α lamellae at the expense of the β ones; (ii) a slow progressive tilting of the lamellae; (iii) a sudden acceleration of the tilting, generally accompanied by a transient pinching of the α lamellae. These three stages of the transient take typically 10 s. They are followed by a fourth and final state (iv) in which the tilt angle, although essentially stabilized at a large value ($\sim 25°$), undergoes slight variations on a much longer time scale.

We believe that the transition is complete after stage (iii) and that stage (iv) belongs to the dynamics of the already quasistationary tilted state. This claim is supported below. We shall focus on the duration of the transient, i.e., the period of time covering stages (i)–(iii), called the transition delay δ thereafter. We shall not try to understand the transient in detail. The conditions of our experiment are not favorable for such a study, in particular because δ is of the same order of magnitude as the instrumental stabilization time mentioned in Sec. II. Some simple remarks can however be made: First as is apparent in Figs. 5–7, δ varies, sometimes rapidly, along the front; this rules out the possibility that the observed transition delay be of purely instrumental origin. Second, as we shall show shortly, δ decreases when the control parameter of the bifurcation increases above the critical value, which is indeed the behavior expected for an instrinsic transient, whatever its detailed cause. Third, there is a physical time in the system that has the same order of magnitude as δ: the diffusion time over one or two lamellar spacings in the liquid. It seems reasonable that the transient would be scaled by this time. This would ex-

plain why the transition delay does not significantly vary with the absolute value of the post-jump pulling velocity (data not shown), the average value of the lamellar spacing being kept constant in our experiments.

The transition delay varies with x along the front; in some cases (in Fig. 6, for instance), this is manifested by the presence of a wavy white line, which is a contrast effect caused by the pinching of the α lamellae at the end of stage (iii). What is the nature of this position-dependent transient? Is it an invasion, that is, does the tilting of the lamellae occur first at some "weaker" place along the initial pattern and then propagate down the front? Figure 10 shows $\delta(x)$ together with the initial $\lambda_0(x)$ plot, for the case corresponding to Fig. 6. There is clearly a strong correlation between the local values of the two functions. Eliminating the x variable leads to the $\delta(\lambda_0)$ relation shown in Fig. 11; a $\phi(\lambda_0)$ relation also exists, which we shall discuss later on.

This result can be cross-checked in the following way, which requires no knowledge of the exact moment of transition. The conservation of the number of lamellae during the course of the transition entails a definite relation between the gradient of δ, λ, and ϕ before (state 0) and immediately after (state $T0$) the transient, which reads as [3]

$$\frac{d\delta}{dx}=[\lambda_{T0}(x)-\lambda_0(x)]/\{\lambda_0(x)\tan[\phi_{T0}(x)]\}\ , \qquad (1)$$

where it has been supposed that $\phi_0=0$. λ_0, λ_{T0}, and ϕ_{T0} can be measured as functions of x and then $d\delta/dx$ calculated from Eq. (1). However, in applying such a formula, we are of course limited by the experimental uncertainties on λ and ϕ (~ 0.2 μm and $\sim 0.5°$, respectively), so that we must content ourselves with a qualitative exploitation. Within experimental uncertainty, one can certainly take, in Eq. (1), $\lambda_0(x)\tan[\phi_{T0}(x)]$ constant, i.e., consider $\lambda_{T0}(x)-\lambda_0(x)$ to be proportional to $d\delta/dx$. Now it can be seen in Fig. 10 that $\lambda_{T0}(x)-\lambda_0(x)$ is roughly proportional to $d\lambda_0/dx$ (in particular, the signs of both quantities change at the same places). The same relation was found in all other cases. Thus, within experimental uncertainty, $d\delta/dx$ is found to be proportional to $d\lambda_0/dx$, in agreement with the results shown in Fig. 11.

In conclusion, the transient cannot be of the invasion type: were that the case, the tilting would probably start where the lamellar spacing is the largest, as observed here, but then propagate with a velocity (equal to $Vd\delta/dx$) varying as a function of $\lambda(x)$. This is not what is observed: the transition delay, not its gradient, is a function of $\lambda(x)$. Apparently, one or two pairs of lamellae are sufficient to constitute a local system behaving more or less independently of the neighboring ones. We shall thereafter refer to this fact as the (pronounced) local character of the bifurcation. Further information on this somewhat surprising aspect of the dynamics is given below.

C. Imperfection of the bifurcation

It can be seen in Fig. 5 that the drifting of the pattern in the final state goes either to the left ($\phi>0$) or to the right ($\phi>0$), or even does not occur, depending on the region considered along the front. This can be very easily explained on the basis of our previous observations concerning the role of surface-tension anisotropy [21]. For instance, it is clear that the field shown in Fig. 5 contains four different eutectic grains. This can be seen from the instabilities attached to the boundaries (lamellar deaths in a row at the 2–3 converging boundary, oscillations and evanescent tilt domains at the 1–2 and 3–4 diverging boundaries), and confirmed by the fact that the basic-state anisotropy-driven tilt angle is different in the different grains. The values of ϕ_0 for the grains of Fig. 5 are given in the caption of this figure. It appears that the

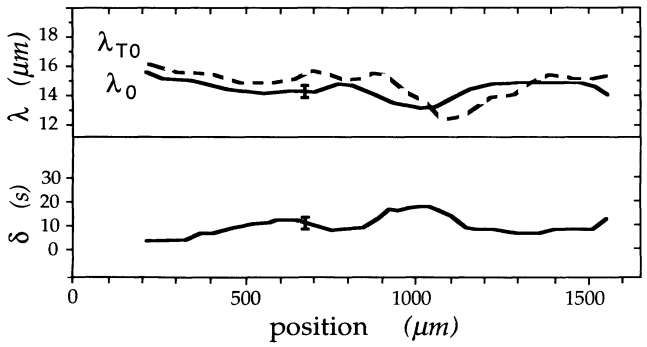

FIG. 10. Initial (λ_0) and post-transition (λ_{T0}) lamellar spacing, and transition delay (δ) against position. Same region as in Fig. 6.

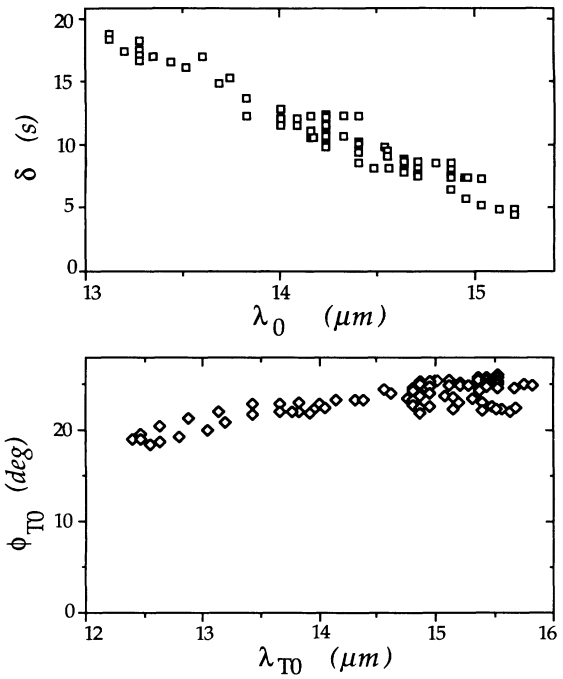

FIG. 11. Transition delay $\delta(x)$ against initial lamellar spacing $\lambda_0(x)$; and tilt angle $\phi_{T0}(x)$ against post-transition lamellar spacing λ_{T0}. Same region as in Fig. 6.

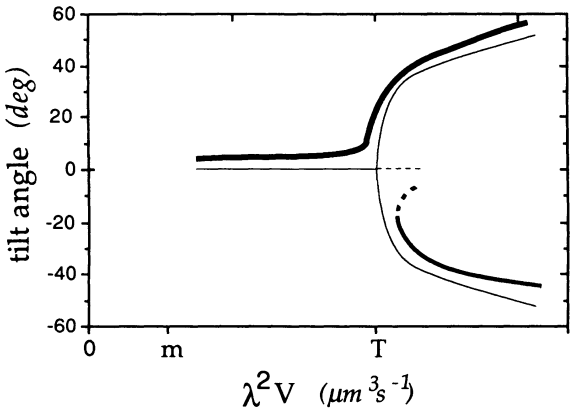

FIG. 12. Probable form of the tilt bifurcation under the effect of capillary anisotropy ($\phi_0 > 0$).

direction (right or left) chosen by the system for the tilt bifurcation is unambiguously determined by the sign of ϕ_0.

It is natural to infer from this observation that, in a system with surface-tension anisotropy, the tilt bifurcation is imperfect. The plausible form of the bifurcation is sketched in Fig. 12 [28]. The continuous branch (at $\phi > 0$ in Fig. 12) accounts for the observed transition, while the isolated branch (at $\phi < 0$) is not observed in the experiments reported here.

The available data do not allow us to be more specific on the bifurcation characterization. Actually, the steepness of the bifurcation will probably prevent any accurate experimental study of the shape of the continuous branch near the threshold; such a study would rely on the unrealistic assumption that initial $\lambda(x)$ distributions of width $< 1\%$ can be obtained. Note also that, according to our interpretation, the exact shape is bound to be grain dependent, being determined by the value of the parameters characterizing the surface-tension anisotropy, which varies from grain to grain.

D. The bifurcation threshold

The regions in Fig. 5 where the tilt bifurcation does not occur are those occupied, before the velocity jump, by the λ gradients attached to the grain boundaries. Figure 13 shows the corresponding initial $\lambda_0(x)$ plot. In this figure, specific symbols are given to the pairs of lamellae that do not undergo the tilting at $t > 0$ (this procedure is unambiguous, except for one or two pairs of lamellae at the limit between regions that undergo the tilt and those that do not). The same analysis was performed for the four runs listed in Table I. The results are shown in Fig. 14 as a plot of the quantity $\lambda_0^2 V_2$ (i.e., $\lambda^2 V$ at $t = 0_+$) against x. A lower limit for the transition to occur appears clearly. Within experimental uncertainty, it depends on the value of $\lambda_0^2 V_2$ and not on that of V_2 (the dependence of the results in G/V is not detectable, within experimental uncertainty). We identify it with the (imperfect) bifurcation threshold, in conformity with both the scaling laws and the local character of the bifurcation. An additional support to this identification is given by the obvious similarity between the process that takes place after a subcritical velocity jump, illustrated in Fig. 9, and the one visible in the region attached to the 2–3 grain boundary in Fig. 5.

The threshold for the tilt bifurcation determined by this procedure is

$$(\lambda^2 V)_T = 680 \pm 40 \ \mu m^3 s^{-1} . \quad (2)$$

The relatively small scatter ($< 10\%$) indicates that surface-tension anisotropy hardly shifts the threshold. The value found for $(\lambda^2 V)_T$ is to be compared with the minimum-undercooling value $(\lambda^2 V)_m$. The evaluation of the latter is difficult and will be discussed elsewhere [19]. For $\eta = 0.5$, our current best estimate is

$$(\lambda^2 V)_m = 190 \pm 20 \ \mu m^3 s^{-1} \quad (3)$$

(for $V = 0.85 \ \mu m \, s^{-1}$, $\lambda_m \cong 14.5 \ \mu m$; note the compatibility with the histograms in Fig. 4). So, we find

$$(\lambda^2 V)_T / (\lambda^2 V)_m = 3.7 \pm 0.6 . \quad (4)$$

This value is clearly compatible with those calculated by Kassner and Misbah [16].

The upper limit of the $\lambda^2 V$ window for the tilt bifurcation that appears in Fig. 14 does not reflect an intrinsic property of this bifurcation. It is, however, interesting, as an example of the interplay between several modes of instability, a situation which seems typical of the dynamics of our system (see Ref. [13] and paper II). It can be seen in Fig. 5, and more clearly in Fig. 15, that the regions with the largest lamellar spacings are oscillating before the velocity jump. This oscillating regime with twice

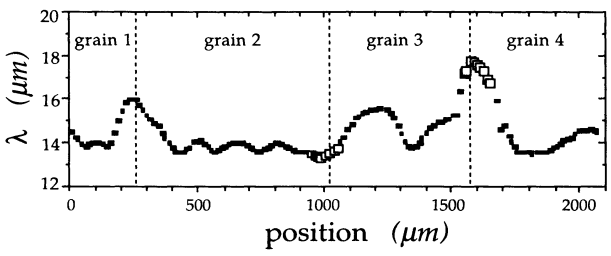

FIG. 13. Initial distribution of lamellar spacings of the region shown in Fig. 5. Open squares: lamellae that do not tilt after the velocity jump.

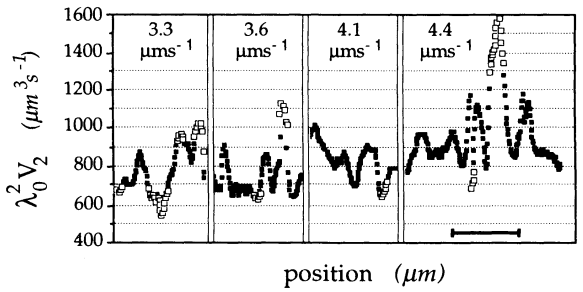

FIG. 14. Plot of quantity $\lambda_0^2 V_2$ against position (bar: 10^3 μm), for the four runs listed in Table I. Inset: values of V_2. Open squares: as in Fig. 13.

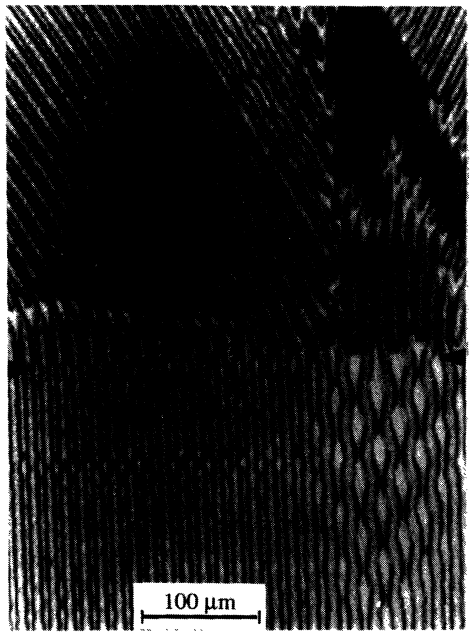

FIG. 15. Enlarged view of the region of Fig. 5 where the vacillating mode is present in the initial state.

the basic wavelength (the 2λ-oscillating [13], or vacillating-breathing [29] mode) is already known to occur in our system when the wavelength of the basic pattern is substantially larger than λ_m. The result of the velocity jumps in these oscillating regions is that the local lamellar-birth instability (see Sec. II) is triggered, decreasing the local lamellar spacing below the critical value for the tilt bifurcation. Thus, the upper limit of the $\lambda^2 V$ window in Fig. 14 is actually the lower threshold of the vacillating mode in the basic state; for $\eta=0.5$ and $V=0.85$ μm s^{-1}, it is at $\lambda \cong 1.2\lambda_m$.

E. Stability and phase dynamics of the extended tilted state

Fauve, Douady and Thual [30] have suggested that extended tilted states may be unstable to long-wavelength perturbations near the bifurcation threshold. Within the experimental limitations explained in Sec. II, we have found that the extended tilted states that are reached by means of velocity jumps have from the onset a nonuniform $\lambda(x)$ distribution inherited from the preexisting basic state (the λ_{T0} distribution of Fig. 10). Figure 16 shows how this λ distribution evolves, in the tilted state. In this figure, λ is plotted against position in the frame drifting at the average drift velocity of the pattern. It can immediately be seen that apart from a hardly significant attenuation of its amplitude, the λ modulation shifts without deformation with respect to this frame. Thus, the width of one particular pair of lamellae, corresponding to points having the same abscissa in Fig. 16, changes relatively rapidly. However, a rigid shift of the distribution does not mean that any phase diffusion is taking place but rather that the evolution is entirely driven by the rapid adjustment of ϕ to the local value of λ [31]. Thus, a natural assumption is that $\phi(x)$ is always near the stationary value $\bar{\phi}[\lambda(x)]$. Clear-cut experimental confirmation of such a conclusion obviously cannot be obtained because of the large experimental uncertainty of the local values of ϕ, and because ϕ is grain dependent; confirmation is, however, further supported by the following observations: Figure 11 shows a series of measured values of the local tilt angle versus local lamellar spacing in a given grain and at a given time. Several series of such measurements are shown in Fig. 17 (for clarity, the individual measurements have not been plotted: all the measurements made in a given grain and at given V, but at different times, are presented by an area with a specific hatching). In spite of the data scatter, the two expected trends clearly emerge: namely, the sensitivity of ϕ to crystal anisotropy, and, within a given grain and at a given pulling velocity, the increase of ϕ with $\lambda^2 V$ following a law similar to the calculated stationary $\bar{\phi}(\lambda)$ law. Whether ϕ really decreases at fixed $\lambda^2 V$ as V increases (see Fig. 17) is not certain, since the series of measurements at different velocities also correspond to different eutectic grains.

In summary, the transition is local primarily as a result of the overall ineffectiveness of phase diffusion in our system. More specifically, the diffusion of the phase along the front over distances of the order of a few λ is extremely slow compared to the ≈ 10 s necessary for the front profile to readjust itself over the same distances. What is striking is that this holds true in spite of the

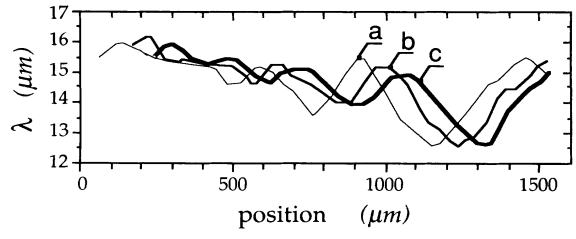

FIG. 16. Evolution of the $\lambda(x)$ distribution in the tilted state, in the reference frame attached to the lamellae. Curves *a*, *b*, and *c*: 200, 300 and 400 s after the transition. Same region as in Fig. 6.

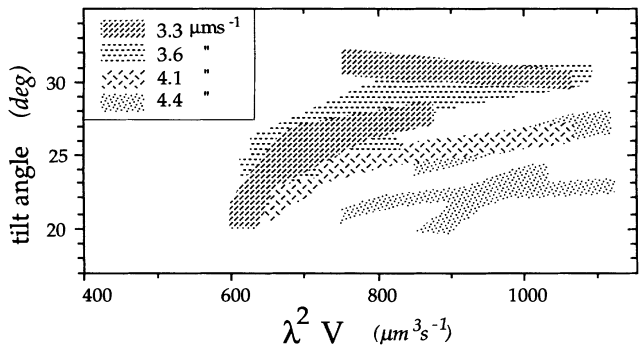

FIG. 17. Local tilt angle $\phi(x)$ against local $\lambda^2 V(x)$. One area represents a series of measurements performed in a given eutectic grain at a given pulling velocity (see inset).

large amplitude of the λ (and thus ϕ) modulations. On the other hand, the slowness of the phase diffusion does not allow any definitive conclusion about the phase stability of the extended tilted state; however, the evolution in Fig. 16 shows that the state is stable.

IV. CONCLUSION

The main conclusions of this work are as follows.

(1) The good agreement between the observations presented here and the theoretical results of Kassner and Misbah leaves no doubt about the existence, in lamellar eutectics, of a parity-breaking bifurcation occurring, for a given value of the pulling velocity, at about twice the minimum-undercooling wavelength. The fact that clear experimental evidence of the bifurcation was obtained only by using very thin samples and limiting the concentration range explored, does not invalidate the general validity of the result, but highlights another important aspect of the dynamics (not studied here), namely the frequent and complex interplay between different modes of instability.

(2) The role played by surface-tension anisotropy in breaking the parity symmetry of the pattern is now well understood: It acts as a weak perturbation of a tilt bifurcation which is essentially spontaneous, i.e., which would occur practically in the same way if there was no anisotropy in the solid. Several pieces of evidence of this role have been given above. However, considering the importance given in the metallurgical literature to the question of the epitaxy between the two solid phases [32], it may be useful to insist again on the necessary distinction between "floating" and "locked" eutectic grains. As mentioned, our conclusions about the tilt bifurcation concern the floating grains only, i.e., those grains in which no epitaxy orientation exists between the two solid phases. How can a floating grain in a homogeneously tilted state be distinguished from a locked grain, as the lamellae make a large angle with the pulling direction in both cases (Fig. 18)? The most obvious distinguishing features are as follows. (i) The front shapes are clearly different: In the locked case, the triple-point pinning angles are small, revealing a low surface tension of the solid-solid interfaces (Fig. 18; see also Refs. [8,11]). (ii) During transients, the lamellae are smooth in the floating case, whereas they bear sharp kinks in the locked case (Fig. 18). (ii) A downward velocity jump provokes a smooth return to the untilted state in floating grains (Fig. 8), whereas, in locked grains, the lamaellae retain their slanting direction. Thus, in our system, the distinction between the two types of grains is unambiguous. It may be less clear-cut in other systems, if the minima of the solid-solid interface Wulff plot happen to be shallow cusps or no cusp at all. This is possibly the case of metallic systems where a dynamics which is clearly of the floating-grain type coexists with preferential orientation relations between the two solid phases.

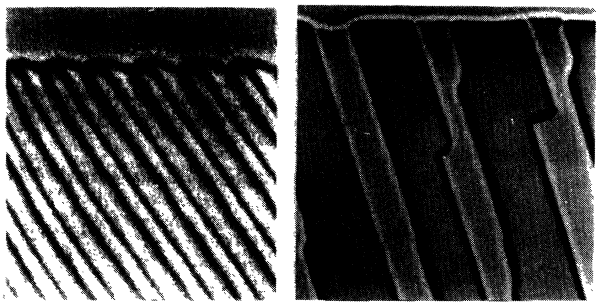

FIG. 18. (a) Floating grain in a homogeneous tilted state ($\lambda \cong 21.5$ μm; $V = 1.54$ μm s^{-1}); (b): locked grain ($\lambda \cong 56$ μm; $V = 3.4$ μm s^{-1}).

(3) An important feature of the dynamics of lamellar eutectics in the pulling velocity range of our experiments is its pronounced local character. This means, first, that phase diffusion is almost absent and relatively large permanent gradients of the lamellar spacing, generated by the boundary conditions, generally present. This fact is not surprising. Phase diffusion was previously observed to be extremely slow in the basic state and an approximate calculation of the phase diffusion coefficient $\mathcal{D}$ showed that for $\lambda \sim \lambda_m$, $\mathcal{D} < 10^{-2} D$ Pe [21]. What is demonstrated here, in addition, is that the tilt angle, thus the front profile, adjusts itself to local conditions (namely, here, to the local value of $\lambda^2 V$) in a short time, which must probably be identified as the chemical diffusion time in the liquid over a distance of the order of a few lamellar spacings.

ACKNOWLEDGMENTS

The authors are glad to acknowledge many enlightening discussions with B. Caroli, C. Caroli, and C. Misbah. They are grateful to C. Guthmann for her help in performing the experiments. They thank R. Mellet (Centre National d'Etude des Telécommunications, Bagneux) for preparing the zone-refined products. This research was supported by the Centre National de la Recherche Scientifique and the Centre National d'Etudes Spatiales. J. M. is financially supported by the Société Péchiney.

[1] J. S. Langer, Phys. Rev. Lett. **44**, 1023 (1980).
[2] A. J. Simon, J. Bechhoefer, and A. Libchaber, Phys. Rev. Lett. **61**, 2574 (1988).
[3] G. Faivre, S. de Cheveigné, C. Guthmann, and P. Kurowski, Europhys. Lett. **9**, 779 (1989).
[4] M. Rabaud, S. Michalland, and Y. Couder, Phys. Rev. Lett. **64**, 184 (1990).
[5] P. Coullet, R. E. Goldstein, and G. H. Gunaratne, Phys. Rev. Lett. **63**, 1954 (1989).
[6] R. E. Goldstein, G. H. Gunaratne, L. Gil, and P. Coullet (unpublished).
[7] B. Caroli, C. Caroli, and S. Fauve, J. Phys. (Paris) (to be published).
[8] J. D. Hunt and K. P. Jackson, Trans. AIME **236**, 843

(1966).
[9] K. A. Jackson and J. D. Hunt, Trans. AIME **236**, 1129 (1966).
[10] J. Bechhoefer, A. J. Simon, A. Libchaber, and P. Oswald, Phys. Rev. **40**, 2042 (1989).
[11] W. L. Kaukler and J. W. Rutter, in *In Situ Composites,* edited F. D. Lemkey, H. E. Cline, and M. McLean (Elsevier, Amsterdam, 1982), p. 30.
[12] V. Seetharaman and R. Trivedi, Metall. Trans. **19A**, 295 (1988).
[13] G. Faivre, C. Guthmann, and J. Mergy, in *Nonlinear Phenomena in Materials Science,* edited by G. Martin and L. Kubin (Trans Tech, Aedermannsdorf, Switzerland, in press), Vol. II.
[14] K. Kassner and C. Misbah, Phys. Rev. Lett. **66**, 445 (1991).
[15] K. Kassner and C. Misbah, Phys. Rev. Lett. **65**, 1458 (1990); **66**, 522 (1991).
[16] K. Kassner and C. Misbah, Phys. Rev. A **44**, 6533 (1991).
[17] The minimal model assumes that the motion of the front is exclusively governed by chemical diffusion in the liquid [see B. Caroli, C. Caroli, and B. Roulet, in *Solids far from Equilibrium,* edited by C. Godrèche (Cambridge University Press, Cambridge, 1992)]. That our system obeys this assumption, i.e., in particular, that there is no convection in the liquid, and no detectable effect due to interface attachment kinetics, has been carefully verified (see Refs. [19,22,23]).
[18] K. Brattkus, B. Caroli, C. Caroli, and B. Roulet, J. Phys. (Paris) **51**, 1847 (1990).
[19] The residual impurity content, including those introduced during the preparation of the samples, has been estimated by measuring the Mullins-Sekerka instability threshold of samples of purified CBr_4. The measurements fall in the range 15–25 $\mu m\,s^{-1}$. For typical values of the impurity-CBr_4 liquidus slope and partition coefficient, this corresponds to impurity concentrations about 10^{-3} mol% [G. Faivre, C. Guthmann, J. Mergy and R. Mellet (unpublished)].
[20] Note that, as the basic-state lamellar spacing is always close to the minimum-undercooling λ_m and $\lambda_m \sim (dl)^{1/2}$, $\mathrm{Pe} \sim (d/)^{1/2}$. Thus, the fact the $\mathrm{Pe} \ll 1$ is also due to $d/l \ll 1$.
[21] B. Caroli, C. Caroli, G. Faivre, and J. Mergy, J. Cryst. Growth **118**, 135 (1992).
[22] S. de Cheveigné, C. Guthmann, and M. M. Lebrun, J. Phys. (Paris) **47**, 2095 (1986).
[23] M. M. Lebrun, thèse, Université Paris 7, 1987 (unpublished).
[24] The fact that, in lamellar eutectics, the lamellar birth occurs by the agency of a localized transverse mode (thus not of tip splitting) was already established by the unpublished observations of J. Van Suchtelen on the thin-film eutectic solidification of binary mixtures of metallic salts (private communication). These observations also contain, in our opinion, pieces of evidence for the tilt bifurcation.
[25] It follows from these remarks that the tilt bifurcation as such will probably never be observed in bulk eutectic samples or in cellular fronts with a low tip-splitting threshold. Although hidden, the bifurcation is nevertheless present in these systems and can manifest itself in associated phenomena, such as tilt domains.
[26] W. Kurz and D. J. Fischer, *Fumdamentals of Solidification* (Trans Tech, Aedermannsdorf, Switzerland, 1984).
[27] J. Mergy, thése, Université Paris 7, 1992 (unpublished).
[28] K. Kassner and C. Misbah have recently performed numerical calculations in a model including surface-tension anisotropy and have found a similar result (private communication).
[29] K. Kassner, C. Misbah, and H. Müller-Krumbhaar, Phys. Rev. Lett. **67**, 1551 (1991).
[30] S. Fauve, S. Douady, and O. Thual, Europhys. Lett. **10**, 309 (1989).
[31] Consider a pattern whose phase $\Phi(x,t)$ shifts rigidly at constant velocity w, i.e, such that $\Phi(x,t)=\Phi(x-wt)$. Then the wave vector $k=\Phi_x(x,t)$ and the drift velocity $V_x=-\Phi_t(x,t)/\Phi_x(x,t)$ are related by $V_x=w/k$.
[32] L. M. Hogan, R. W. Kraft, and F. D. Lemkey, Adv. Mater. Res. **5**, 83 (1971).

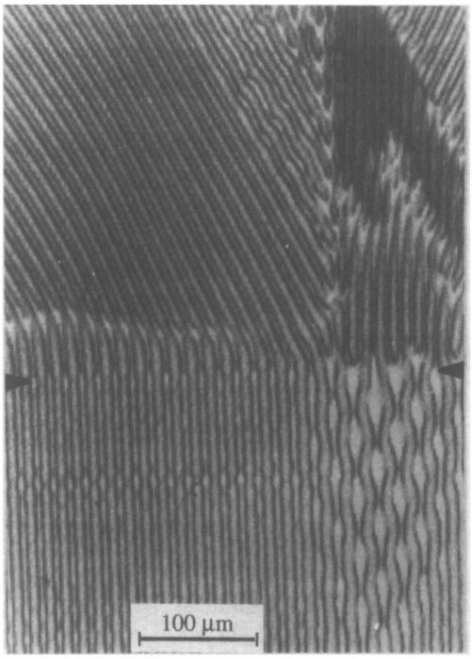

FIG. 15. Enlarged view of the region of Fig. 5 where the vacillating mode is present in the initial state.

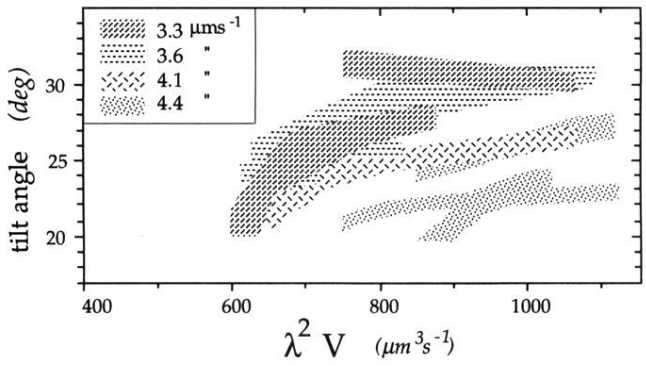

FIG. 17. Local tilt angle $\phi(x)$ against local $\lambda^2 V(x)$. One area represents a series of measurements performed in a given eutectic grain at a given pulling velocity (see inset).

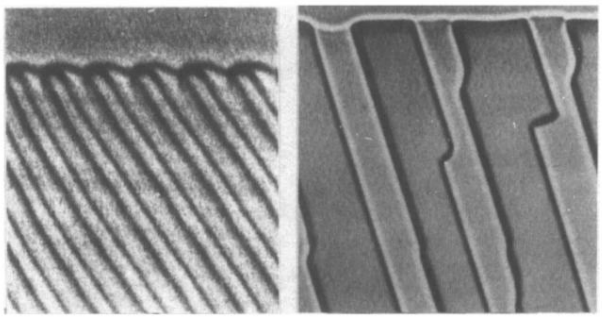

FIG. 18. (a) Floating grain in a homogeneous tilted state ($\lambda \cong 21.5\ \mu$m; $V = 1.54\ \mu\mathrm{m\,s^{-1}}$); (b): locked grain ($\lambda \cong 56\ \mu$m; $V = 3.4\ \mu\mathrm{m\,s^{-1}}$).

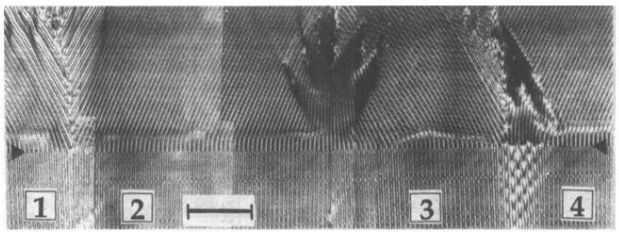

FIG. 5. Velocity jump from $V_1=0.85$ to $V_2=3.6$ $\mu m\,s^{-1}$ (run 2 of Table I). Photograph of the solid (the solidification front is out of the image). Time is running upwards. Arrows: velocity jump ($t=0$). Bar: 200 μm. Numbers 1–4: eutectic grains. The values of ϕ_0 for grains 1–4 are $+3°$, $-2°$, $+2.5°$, $-1.5°$, respectively. An incipient dendritic destablization is visible in the upper left corner as are "sources" emitting tilted lamellae at the 1–2 and 3–4 grain boundaries (sources and other "defects" of the tilted state will be described in paper II).

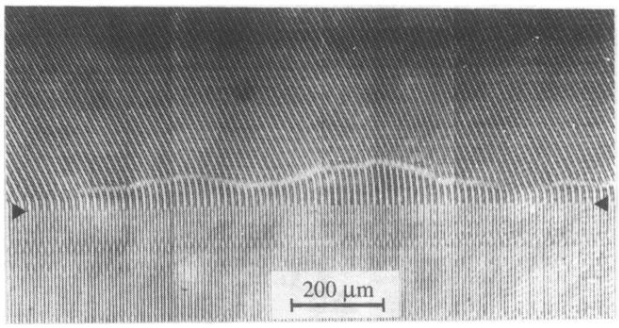

FIG. 6. Velocity jump from $V_1 = 0.85$ to $V_2 = 4.1$ $\mu m\,s^{-1}$ (run 3 of Table I). See Fig. 5 for explanations. Only one eutectic grain is visible in the image ($\phi_0 = +0.5°$).

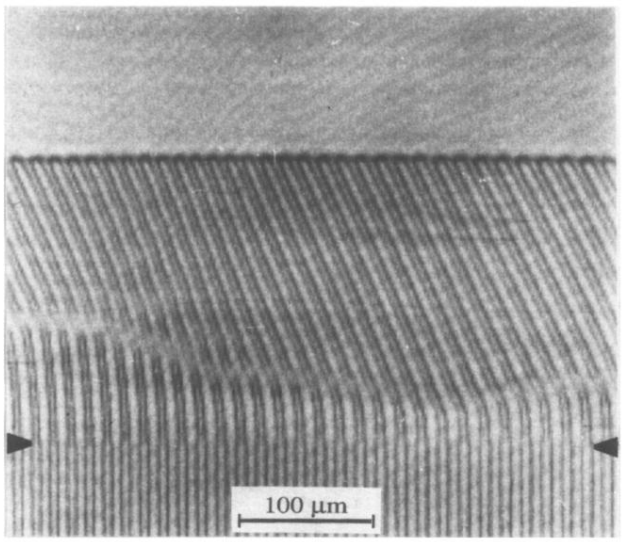

FIG. 7. Enlarged view of the same region as in Fig. 6. The photograph was taken at $t = 65$ s.

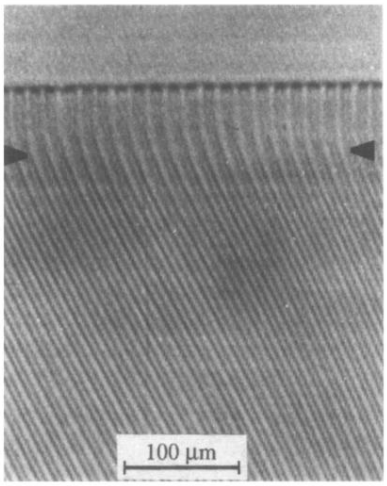

FIG. 8. Velocity jump from 4.1 to 0.85 μm s^{-1} (end of run 3). Arrows: velocity jump.

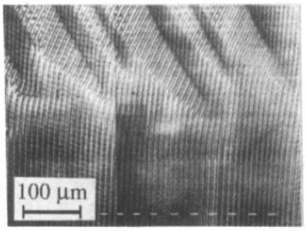

FIG. 9. Subcritical velocity jump ($V_1 = 0.85\ \mu m\, s^{-1}$; $V_2 = 2.26\ \mu m\, s^{-1}$; $R = 2.7$). Dashed line: velocity jump.